On flames established with air jet in cross flow of fuel-rich combustion products

Citation	Katta, V. R., Blunck, D. L., Jiang, N., Lynch, A., Gord, J. R., & Roy, S. (2015). On flames established with air jet in cross flow of fuel-rich combustion products. Fuel, 150, 360-369. doi:10.1016/j.fuel.2015.02.006
DOI	10.1016/j.fuel.2015.02.006
Publisher	Elsevier
Version	Version of Record
Terms of Use	http://cdss.library.oregonstate.edu/sa-termsofuse

Fuel 150 (2015) 360–369

Contents lists available at ScienceDirect

Fuel

journal homepage: www.elsevier.com/locate/fuel

On flames established with air jet in cross flow of fuel-rich combustion products

Viswanath R. Katta [a,*], David L. Blunck [b], Naibo Jiang [c], Amy Lynch [d], James R. Gord [d], Sukesh Roy [c]

[a] Innovative Scientific Solutions, Inc., Dayton, OH 45459, USA
[b] Oregon State University, Corvallis, OR 97331, USA
[c] Spectral Energies, LLC, Dayton, OH 45431, USA
[d] Air Force Research Laboratory, Wright-Patterson Air Force Base, OH 45433, USA

HIGHLIGHTS

- Modeled inverse diffusion flames in fuel-rich combustion products.
- Reacting flow associated with jet-in-cross-flow environment is simulated using a detailed chemical kinetics.
- Predicted the unusual flame movement when the blowing ratio or equivalence ratio was increased.
- Hydrogen in the cracked fuel products causes non-intuitive flame behavior due to preferential diffusion.

ARTICLE INFO

Article history:
Received 3 November 2014
Received in revised form 31 January 2015
Accepted 3 February 2015
Available online 16 February 2015

Keywords:
Jet-in-cross-flow
Film-cooling
Diffusion flame
Autoignition
Preferential diffusion

ABSTRACT

Advances in combustor technologies are driving aircraft gas turbine engines to operate at higher pressures, temperatures and equivalence ratios. A viable approach for protecting the combustor from the high-temperature environment is to inject air through the holes drilled on the surfaces. However, it is possible that the air intended for cooling purposes may react with fuel-rich combustion products and may increase heat flux. Air Force Research Laboratory (AFRL) has developed an experimental rig for studying the flames formed between the injected cold air and the cross flow of combustion products. Laser-based OH measurements revealed an upstream shift for the flames when the air injection velocity was increased and downstream shift when the fuel content in the cross flow was increased. As conventional understanding of the flame stability does not explain such shifts in flame anchoring location, a time-dependent, detailed-chemistry computational-fluid-dynamics model is used for identifying the mechanisms that are responsible. Combustion of propane fuel with air is modeled using a chemical-kinetics mechanism involving 52 species and 544 reactions. Calculations reveled that the flames in the film-cooling experiment are formed through autoignition process. Simulations have reproduced the various flame characteristics observed in the experiments. Numerical results are used for explaining the non-intuitive shifts in flame anchoring location to the changes in blowing ratio and equivalence ratio. The higher diffusive mass transfer rate of hydrogen in comparison to the local heat transport enhances H_2–O_2 mixing compared to thermal dissipation rate, which, in turn, affects the autoignition process. While increasing the blowing ratio abates the differences resulting from non-equal mass and heat transport rates, higher concentrations of hydrogen in the fuel-rich cross flows accelerate those differences.

1. Introduction

Efforts continue to be made to make gas turbine engines smaller, more efficient and operate with reduced environmental impact. Studies [1] have indicated that reheating of the combustion products between the high- and low-pressure turbine stages in a gas turbine engine could improve the specific thrust by as much as 50%. However, as a conventional combustor is too large to be incorporated for generating the extra heat between the two turbine stages, new technologies such as Ultra Compact Combustor (UCC) are being developed. The UCC reduces the length of the system by integrating turbine turning vanes within the combustor [2,3] and incorporating trapped-vortex concepts [4,5]. One challenge to developing UCC technology is providing adequate cooling

* Corresponding author at: Innovative Scientific Solutions, Inc., 7610 McEwen Road, Dayton, OH 45459, USA. Tel.: +1 (937) 255 8781.
E-mail address: vrkatta@gmail.com (V.R. Katta).

http://dx.doi.org/10.1016/j.fuel.2015.02.006
0016-2361/

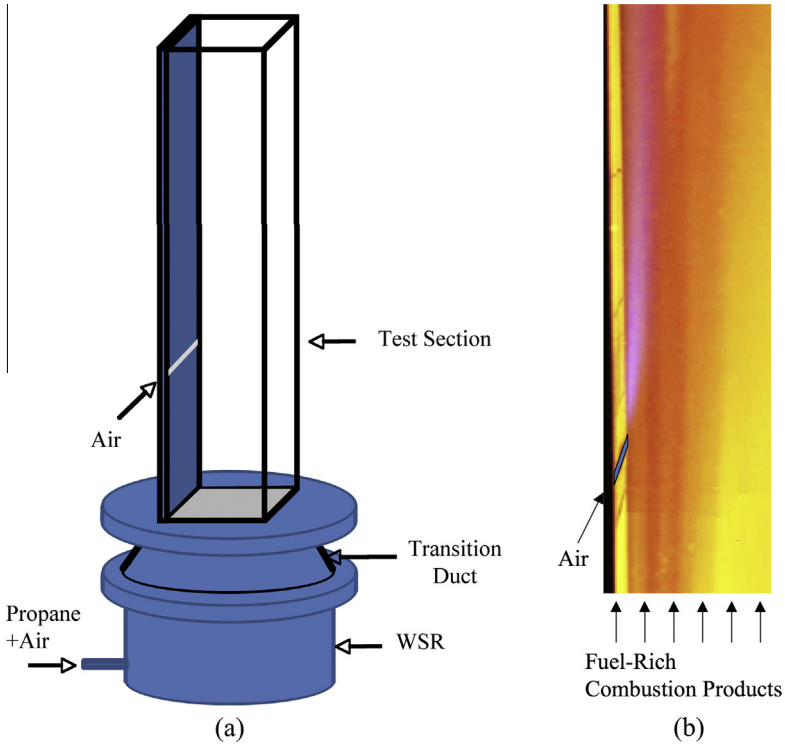

Fig. 1. (a) Schematic diagram of AFRL test rig, (b) direct photograph of the flame formed in the test section.

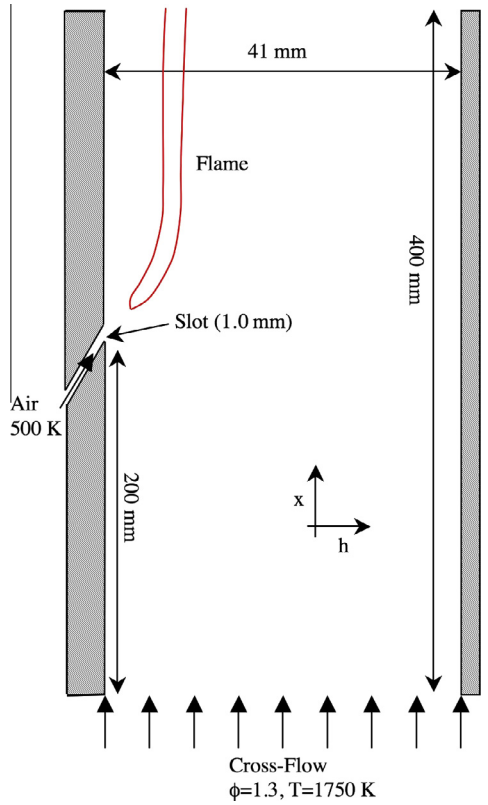

Fig. 2. Two-dimensional view of the test section of AFRL test rig. Left sidewall upstream of the slot is water cooled in the experiment.

for the vanes. A strategy for cooling the surface of vanes is to inject air through the perforations (holes). However, because portions of the vanes are exposed to fuel-rich combustion products there is a potential that the air supplied for cooling may actually react. Hence improperly designed air-cooling may actually increase heat flux to the surfaces. Irrespective of UCC technology, the motivation for increasing cycle efficiency is also pushing the combustors to operate at overall equivalence ratio closer to unity. This increases the opportunity for unburned fuel from the combustor to pass into the turbine section where air intended for cooling may cause flames to form. Reactions near the surfaces can increase temperatures-effectively deteriorating the cooling efficiencies obtained through injecting air [6,7].

Research studying reactions between film-cooling air and incomplete combustion products has typically been limited to quantifying increase in temperature or change in the heat flux near the surfaces [6–9]. For example, studies of Polanka et al. [6] and Kirk et al. [9] compared the heat fluxes resulted from the reacting and nonreacting environments for a range of freestream equivalence ratios and cooling-hole geometries. On the other hand, characterization of the reacting flow (for example, identification of flame and extinction zones) is also needed to help understand the causes for changes in measured heat flux and to help in applying the laboratory findings to practical systems. Two exceptions are the work of Polanka et al. [6] and Lin et al. [10] who performed CFD calculations using two-step reaction scheme. The reaction zone distribution for varying equivalence ratios and freestream conditions was reported. Such studies must be enhanced with measurements and calculations made with detailed chemical

Table 1
Cross-flow description.

ϕ	T (K)	X_{H2}	X_{CO}	X_{CO2}	X_{H2O}	X_{N2}
1.3	1750	0.0333	0.0731	0.0664	0.1521	0.675
1.4	1720	0.0488	0.0899	0.0567	0.1463	0.658
1.5	1670	0.0654	0.1040	0.0492	0.1388	0.642
1.6	1630	0.0999	0.1269	0.0390	0.1211	0.613

kinetics for determining flame anchoring positions and their sensitivity to the operating conditions.

Air injected into a cross flow of fuel-rich combustion products represents an inverse diffusion flame chemically and a jet in cross flow fluid dynamically. The structure (i.e., temperature and species distributions) of an inverse diffusion flame is similar to that of a normal diffusion flame [11–14]. Only limited studies have been made in the past for inverse diffusion flames at conditions that are relevant to gas turbine combustors [15–17]. Similarly, most of the jet-in-cross-flow studies in the past were limited to non-reacting flows. The direct numerical simulations of Muppidi and Mahesh [18] showed that transverse jets entrain significantly more fluid than the normal coaxial jets. Gutmark et al. [19] demonstrated this experimentally through identifying additional vortical structures surrounding the transverse jets. The reacting jet-in-cross-flow studies of Clausing et al. [16] demonstrated the effects of size and temperature of transverse jets on flame stability. On considering the importance of flame stability in reacting film cooling environments, an attempt is made in the present study for understanding the anchoring behavior of inverse diffusion flames formed between transverse air jets and cross flow of combustion products.

2. Burner configuration

Realizing the need for understanding the reactivity of the air jets in a cross flow of combustion products, Air Force Research Laboratory (AFRL) developed a reacting film cooling test rig [6,20]. A schematic diagram of the experimental rig is shown in Fig. 1a. It consists of a rectangular test section and a well-stirred reactor (WSR) for supplying high temperature, fuel-rich combustion products. Premixed fuel (propane) and air are injected into WSR [21] and burned at atmospheric pressure. The combustion products exiting the WSR flowed through a transition duct and then through the film cooling test section. A transition duct is placed between the circular exit of the WSR and the rectangular test section. Flow straighteners are installed at the base of the transition duct for straightening the swirling flow exiting the WSR. The transition duct is covered with ceramic material for minimizing heat losses.

The film cooling test section consists of an instrumented flat wall plate on one side and quartz windows on the other three sides. The wall plate is water cooled to ensure that the material does not warp or ablate. A rectangular slot is machined into the wall plate for inserting various injection schemes such as a group of circular jets, a rectangular jet, etc. Each insert was designed with hollow, capped cavity to create a plenum for the air supply. The supplied cooling air at room temperature gets convectively heated as it passes through the insert reaching a temperature of ~500 K. The test section is equipped with thermocouples for temperature measurements and Nd:YAG pumped dye lasers for measuring OH mole fractions with planar-laser-induced-fluorescence (PLIF) technique. Details of the measurements and the experimental arrangement are provided in Ref. [22].

A slot (two-dimensional) injection scheme is considered in this study. A direct photograph of the flame formed in the test section is shown in Fig. 1b. It is a very weak flame with light blue visible light emission. Flame is located very close to the wall and, most likely, within the boundary layer. It is very stable and anchored a few mm downstream of the slot. The hot combustion products entering the test section heated up the metal surfaces and caused visible radiation (yellow to orange). The quartz windows are also reflecting this light. Even though the fuel used in this study is propane, very little soot was generated in the test section, probably due to the short residence times (~2 ms).

The cross-sectional geometry of the test section used in the model is shown in Fig. 2. Combustion products from WSR are fed into the test section as a cross flow at ~25 m/s. Fresh air is injected into the test section from the left wall through a 1.0-mm (at the exit) slot hole that was made between $x = 200$ and 201 mm at an

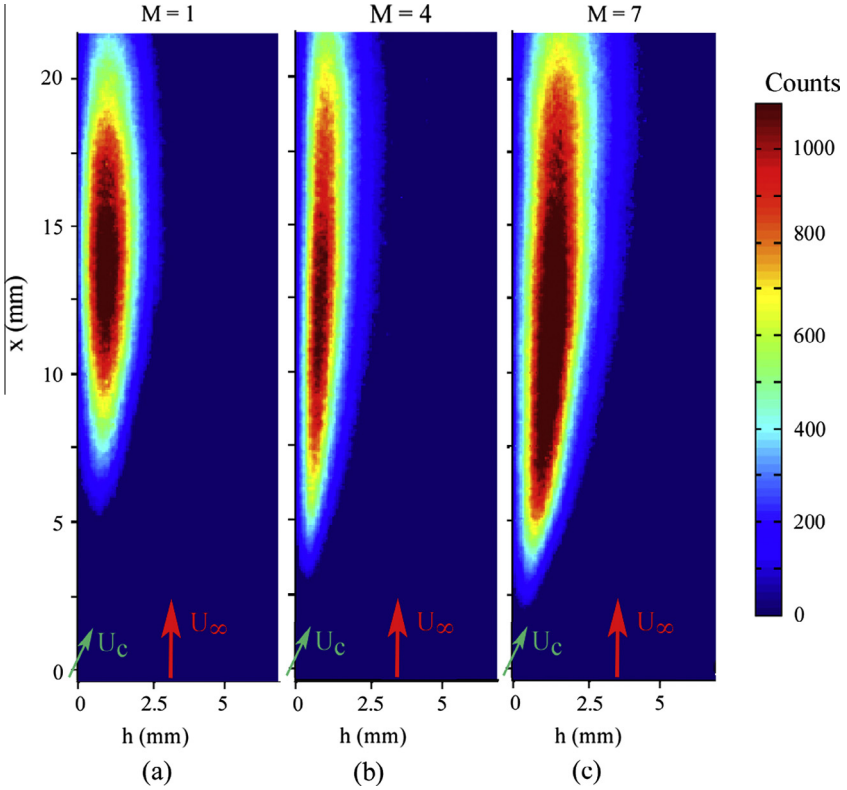

Fig. 3. OH images obtained for blowing ratios (a) 1.0, (b) 4.0 and (c) 7.0.

angle of 30 degrees. The measured temperatures of the air and fuel-rich flow entering the test section were used as boundary conditions in the simulations. While the temperature of the cooling air was set at 500 K for all the cases, the temperature of the cross flow changed with equivalence ratio. The four equivalence ratios considered in this study and the corresponding WSR exit temperatures are given in Table 1. The composition of the gas exiting the WSR was estimated using an equilibrium code and is assumed to be the same at the entrance of the test section. Note that the residence time in the WSR was sufficient for yielding exhaust products (especially, the major species) very close to the equilibrium values. All the minor species with concentrations below 0.5% were ignored for making the boundary conditions well defined. Note that the adiabatic temperatures of the cross flow are about 200 K higher than the measured values. The differences are attributed to the heat loss within the WSR.

3. Computational model

Simulations for the reacting flowfields in AFRL film-cooling test rig are performed using UNICORN code [23–26]. UNICORN is a time-dependent, two-dimensional mathematical model developed for the simulation of unsteady reacting flows. It is capable of performing simulations for laminar and turbulent flames and has been developed over a ten-year period. Its evolution has been in conjunction with experiments conducted to test its ability to predict ignition, extinction, stability limits, and the dynamic characteristics of nonpremixed and premixed flames of various fuels. It solves for u- and v-momentum equations, continuity, and enthalpy- and species-conservation equations on a staggered-grid system. A clustered mesh system is employed to resolve the large gradients in flow variables near the flame surface. A semi-detailed, chemical-kinetics model developed at University of California at San Diego [27] for the combustion of propane is incorporated. The mechanism consists of 52 species and 544 reactions and is listed in the Supplementary material. Earlier studies [28] using this mechanism suggested that it is reasonable for computing structures of various diffusion and partially premixed flames. Thermo-physical properties such as enthalpy, molecular viscosity, molecular thermal conductivity, and binary molecular diffusion of all the species are calculated from the polynomial curve fits developed for the temperature range 300–5000 K. The laminar mixture viscosity and thermal conductivity are then estimated using the Wilke and Kee expressions, respectively. Molecular diffusion is assumed to be of the binary-diffusion type, and the laminar diffusion velocity of species is calculated using Fick's law and the effective-diffusion coefficient of that species in the mixture.

The finite-difference forms of the momentum equations are obtained using an implicit QUICKEST scheme [24], and those of the species and energy equations are obtained using a hybrid scheme of upwind and central differencing. At every time step, the pressure field is accurately calculated by solving all the pressure Poisson equations simultaneously and using the LU (Lower and Upper diagonal) matrix-decomposition technique. The implementation of various boundary conditions is described in Ref. [29].

The computational domain between the walls in Fig. 2 was discretized using a non-uniform grid system of 601 × 251. The minimum grid spacing achieved near the base of the flame formed around the air jet was 50 μm. Simulations presented here were performed on a single cpu, Intel i7-920 Personal Computer with 2.0 GB of memory. Typical execution time is ~20 μs/time-step. Steady state solutions are typically obtained in about 50,000 time steps (0.1 s real time) starting from the solution obtained using a global combustion chemistry model. These large numbers of time steps are needed for an accurate development of the boundary layer.

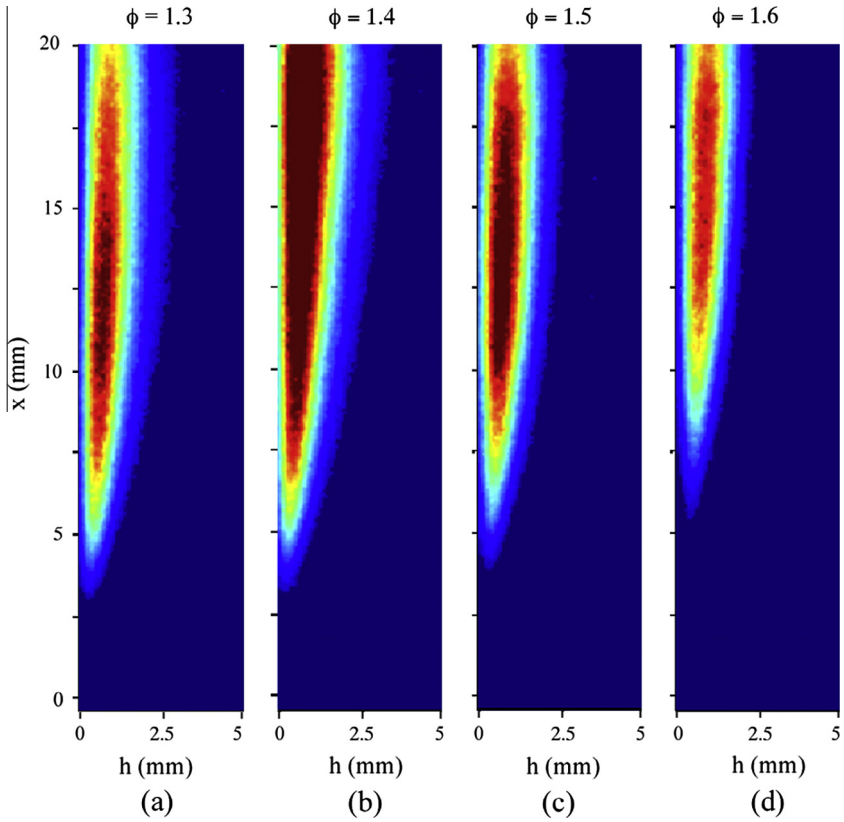

Fig. 4. OH images obtained for cross-flow equivalence ratios (a) 1.3, (b) 1.4, (c) 1.5, and (d) 1.6.

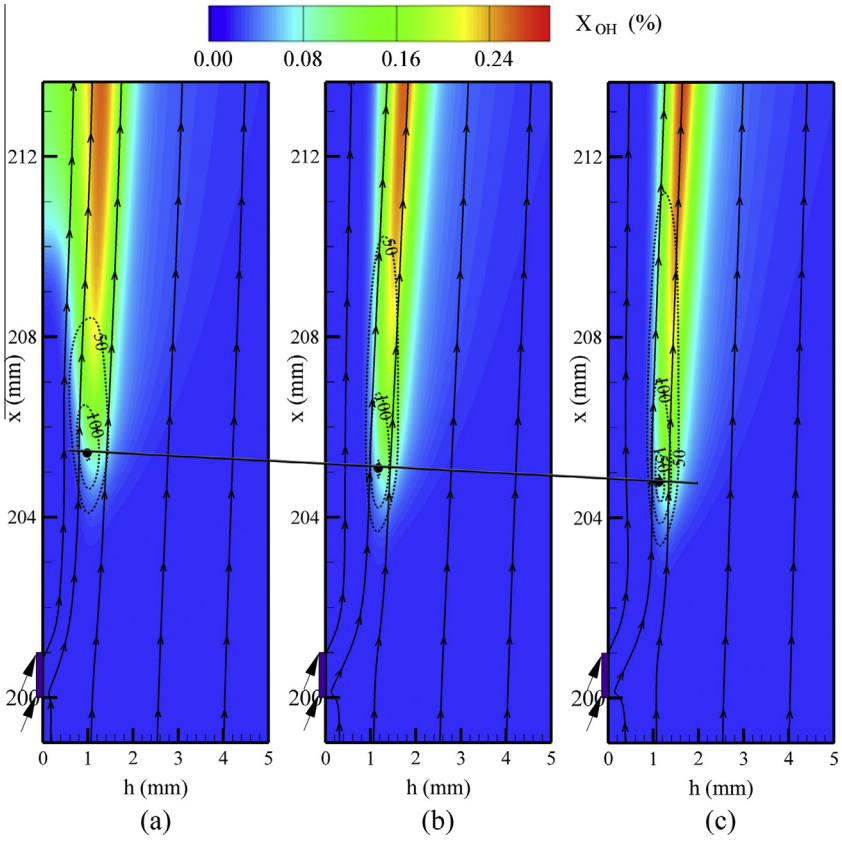

Fig. 5. Flames computed for blowing ratios of (a) 1, (b) 4 and (c) 7. Streamlines (solid lines) and iso-contours of heat release rate (broken lines) are superimposed on OH concentrations. Black dots represent peak heat release rate locations.

The cross-flow velocity of 25 m/s suggests a turbulent flow in the test section. However, as the cross-flow gas temperature is ~1700 K, the velocity based on cold-flow Reynolds number is only 3 m/s; which suggests a laminar or transitional flow. Recent laminar and turbulent calculations [32] performed for this rig using k–ε turbulence model further suggests that the flows are mostly laminar.

4. Results and discussion

A parameter that is often used for characterizing the film-cooling conditions is the blowing ratio [30], which is defined as

$$M = \frac{\rho_c U_c}{\rho_\infty U_\infty}. \quad (1)$$

Here, ρ and U represent density and velocity, respectively and the subscripts c and ∞ represent cooling flow from the holes and the fuel-rich cross flow from WSR, respectively. In non-reacting flows it is obvious that higher blowing ratios yield greater cooling for the wall downstream of the injection holes, as along as the film remains attached to the wall. However, in reacting flows, effects of blowing ratio on wall cooling depends on the characteristics of the flames established between the injected air and fuel-rich cross flow.

Experiments for AFRL test rig with slot injection hole were conducted for different blowing ratios and equivalence ratios. Time-averaged OH images obtained with the PLIF technique [22] are plotted in Fig. 3 for three blowing ratios (M = 1, 4 and 7). Here, the cross-flow equivalence ratio (ϕ) and velocity (U_∞) were fixed at 1.3 and 25 m/s, respectively. The blowing ratio was varied through changing the velocity (U_c) of the cooling air injected from the slot. The line at h = 0 represents cooling plate and that at x = 0 represents cross-section of the test rig at the leading edge of the slot. The average OH emission in Fig. 3 suggests that flames have been established for all the blowing ratios considered. Note that no external source of ignition was provided. Faint blue radiation from flames was also observed with naked eyes for all the cases. The OH images shown in Fig. 3 were not corrected for the temperature or molar densities, hence, represent relative concentrations. It is also imperative that the peak concentration in one image has no relationship with those in the other two images. Nevertheless, the time-averaged OH images in Fig. 3 give qualitative information regarding the flame structure. The following observations are made:

- In general, flames are thin (~2.5 mm) and seem laminar. Shot-to-shot measurements (not shown) did not reveal significant variations in OH fluorescence.
- Flames are not anchored to the slot. They are formed significantly away from the slot's trailing edge (x = 1.0 mm).
- Flame anchoring location shifted upstream with increasing blowing ratio.
- Flame moved away from the wall as the blowing ratio is increased.

Conventional understanding about jet diffusion flames (regular or inverse) suggests that the flame anchoring location should shift downstream with increase in jet velocity [31]. However, the flames in AFRL test rig shifted upstream as the jet velocity was increased. Such a non-intuitive shift in flame location is not limited to cross-flow equivalence ratio of 1.3. Experiments performed with

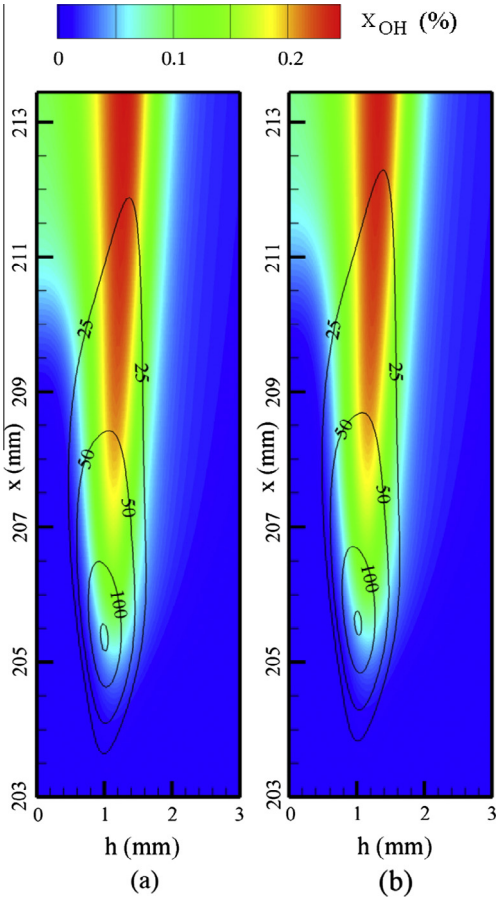

Fig. 6. Flame for blowing ratio of unity computed with two different grid systems. (a) Grid system of 601 × 151 used in the present work and (b) a finer system of 1201 × 301 used for demonstrating the accuracy of the flame computed with the former.

different equivalence ratios (1.3–1.8) also revealed similar trends. As the velocity of the cross flow was kept constant for all the cases, the boundary layer growth on the side walls should not influence the observed flame shift with blowing ratio.

Experiments conducted at a fixed blowing ratio suggested that the flame anchoring location shifts downstream when equivalence ratio is increased. OH images obtained for different equivalence ratios with a blowing ratio of 4 are shown in Fig. 4. Such a shift in flame anchor location when the equivalence ratio was increased is also not as expected. Note that the equivalence ratio used in this study represents the fuel-air ratio entering the WSR. Most of the fuel and all of the air was burned in WSR and only leftover fuel (in the decomposed form) along with the products enters test section. This excess fuel mixes with the air issued from the slot and forms a flame. Therefore, one should not correlate the burning velocities of the initial fuel–air mixtures to the anchoring location of the diffusion flames. A more appropriate variable for characterizing the cross flow is fuel dilution ratio, which represents the ratio between the fuel and products concentrations. Fuel dilution ratio decreases with equivalence ratio. Typically, a diffusion flame moves upstream when the fuel dilution is decreased (or increase in ϕ). However, the flame in the test rig moved downstream with ϕ (Fig. 4). The unique responses of the flame to the variations in blowing ratio and equivalence ratio are studied further using numerical simulations.

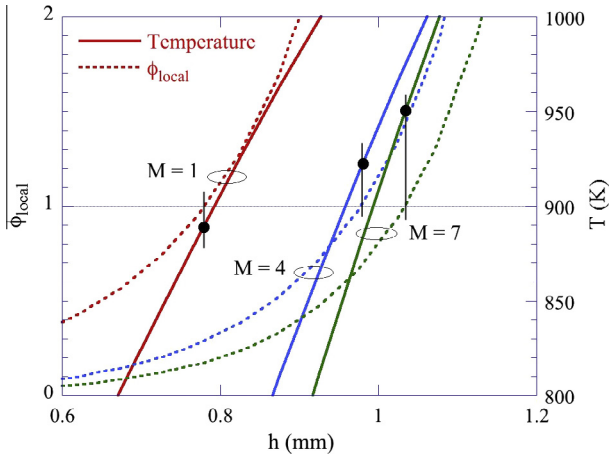

Fig. 7. Cross-sectional distributions of temperature and local equivalence ratio at $x = 202.5$ mm in flames formed with different blowing ratios. Temperatures at stoichiometry ($\phi_{local} = 1$) are marked with black circles.

Laminar, two-dimensional calculations for the test rig are performed for different blowing-ratio and equivalence-ratio conditions. While the velocity for the cross flow was set at 25 m/s to match with the experiments, the velocities for the injection jet were calculated based on blowing ratios, densities and a correction factor. The blowing ratios specified in the experiments were obtained from Eq. (1) with the velocities that were estimated from the mass flow rates and areas. While the estimation of cross-flow velocity was straightforward, estimation of cooling air velocity requires some understanding of the geometry. As the slot hole is inclined at an angle of 30 degrees with respect to the wall surface, the width of the slot at the exit is twice larger than the actual slot hole. Moreover, as the slot in the experiment was not extended all the way to the sidewalls (in the direction normal to x and h in Fig. 2), a reduction in jet velocity by 20% was needed for 2-d modeling (allowing the assumption of slot extending to the sidewalls). Considering the differences in the slot widths and lengths used in the experiment and model, velocities for the injection jets were determined after reducing the values estimated from blowing ratios by a factor of 2.5 as follows:

$$U_c = 0.4 * M\rho_\infty U_\infty/\rho_c. \quad (2)$$

Note that the mass flow rates used in the simulations matched exactly with those used in the experiment and U_c is in the direction parallel to the slot hole. The wall at $h = 0$ was cooled between inlet and slot and its surface temperature (610 K) was measured at a location a few mm upstream of the slot. In the absence of a detailed distribution, a simple linear variation from inlet temperature (given in Table 1) to 610 K was applied as boundary condition to the bottom wall in the calculations. The wall downstream of the slot ($x > 201$ mm) was treated as an adiabatic wall.

4.1. Effect of blowing ratio

Flame structures computed for three blowing ratios (1, 4 and 7) are shown in Fig. 5. Here, streamlines and iso-contours of heat release rate are superimposed on OH concentration distributions. Locations where heat release rate peaks are marked with black circles. Note, similar to experiments, no separate ignition source was provided in the calculations for obtaining these flames. The high gas temperature was sufficient for igniting the fuel–air mixture downstream of the slot. Similar to normal jet diffusion flames heat release rate peaked near the flame base. Computed peak OH concentration is located between 1 and 2 mm away from the sidewall. This separation is similar to that observed in the experiments (Fig. 3).

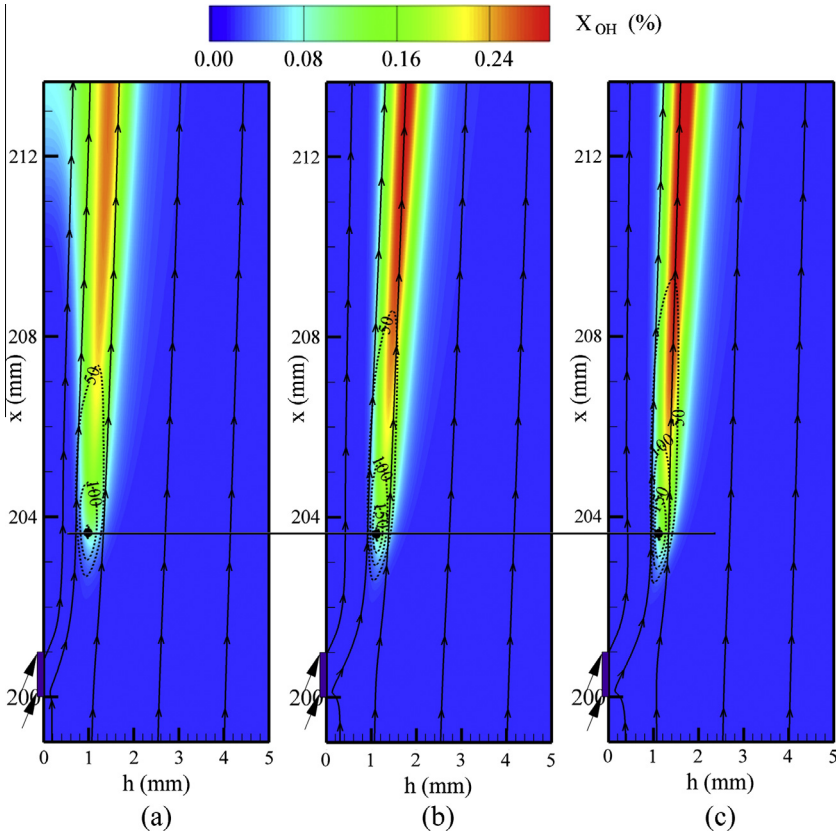

Fig. 8. Flames computed after assuming diffusivities of all the species are equal. Blowing ratios are (a) 1, (b) 4 and (c) 7. Streamlines (solid lines) and iso-contours of heat release rate (broken lines) are superimposed on OH concentrations. Black dots represent peak heat release rate locations.

Fig. 5 suggests that the flames are lifted and anchored about 3 mm downstream of the injection slot. These results are qualitatively in good agreement with the experimental data shown in Fig. 3. Note that the leading edge of the slot is at $x = 0$ in the experimental images (Fig. 3) and at $x = 200$ mm in the computed images (Fig. 5). Because of the high temperature (~1750 K) of the fuel-rich gases spontaneous ignition of the fuel is expected when it mixes with air. However, as shown in Figs. 3 and 5, flames in both the experiments and computations are anchored a few millimeters downstream of the injection jet. As previously mentioned the wall upstream of the slot hole was water cooled, which reduced the temperature of the fuel-rich gases near the wall and delayed the autoignition process.

Simulations predicted the flame's upstream movement when the blowing ratio was increased. While the flame in the calculations shifted only about 0.6 mm (based on peak-heat-release-rate location), it has shifted nearly 3 mm (based on OH concentration) in the experiment. The smaller shift in the calculation could be resulting from the semi-detailed chemistry model used in the present study. It is known that the low-temperature chemistry (important for ignition) is often compromised while reducing the chemical-kinetics models for combustion. Nevertheless, the upstream shift predicted in the simulations, which is inline with the experiments, is counterintuitive and must be understood.

Calculations in Fig. 5 were repeated with a finer grid system for eliminating the possibility that the adopted grid system (50-μm resolution) might have artificially caused an upstream shift in the flame location when the blowing ratio was increased. Flames obtained for $M = 4$ case with the standard grid (601×151) and refined grid (1201×301) are shown in Fig. 6a and b, respectively. The latter grid has a resolution of 25 μm in both the x and h directions. Fig. 6 demonstrates that nearly the same flame structure is obtained with both the grid systems. A slight shift in heat-release-rate distribution was noted in the flame simulated with the finer grid. It is believed that more points near the wall in the finer-grid simulations in Fig. 6b resolved the thermal boundary layer slightly better and delayed the autoignition process by ~0.25 mm. Identical shifts in autoignition were also observed in the finer-grid simulations for the other two cases of $M = 1$ and 7 when compared to their counterparts in the standard-grid simulations. These simulations suggested that the noted upstream shift in flame-anchor location with blowing ratio is grid independent.

To understand the upstream shift of flame with blowing ratio several parameters associated with the flame base are investigated. Velocity and heat release rate at the peak heat-release-rate locations (black dots in Fig. 5) are found to increase with blowing ratio. Temperatures at these locations are nearly the same. All of these observations suggest that the flame should have moved downstream rather than upstream when the blowing ratio was increased [31]. To understand this unusual flame behavior better, flow variables upstream of the flame base are compared for the three blowing ratio cases. Cross-sectional distributions of temperature and local equivalence ratio at $x = 202.5$ mm are plotted in Fig. 7. This location is about half way between the trailing edge of the slot and the peak-heat-release-rate location. Here, the local equivalence ratio is calculated based on the fuel and oxygen mole fractions present locally. Table 1 suggests that H_2 and CO fuels are present in the cross flow. Hence, both of these species are used in the local equivalence ratio calculations. Temperatures at stoichiometry ($\phi_{local} = 1$) are marked with black circles in Fig. 7 for the three blowing-ratio cases. As the blowing ratio is increased, stoichiometric location shifted away from the wall and the local temperature at this location increased. These trends can be understood by following the flowfields.

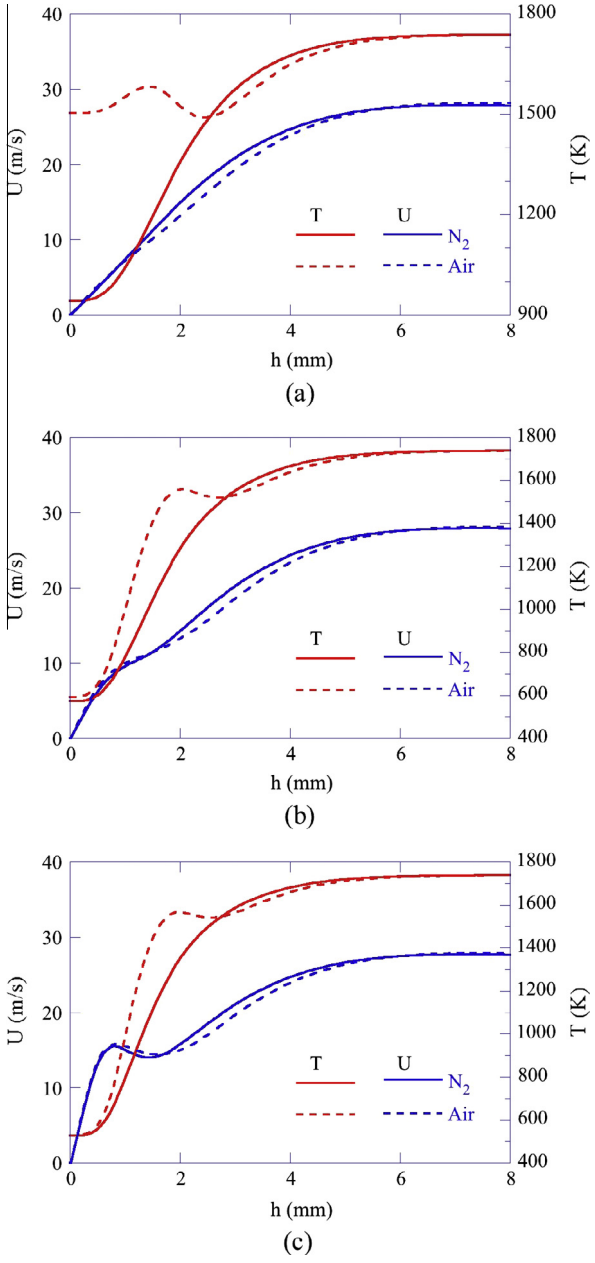

Fig. 9. Cross-sectional distributions (at $x = 215$ mm) of temperature and longitudinal velocity computed with air (broken lines) and nitrogen (solid lines) injections at blowing ratios of (a) 1, (b) 4 and (c) 7.

The flowfields downstream of the slot (Fig. 5) suggest that fuel components such as H_2 and CO from cross flow diffuse toward the wall, heat of the cross flow conducts toward the wall into the cooling jet, and oxygen in the cooling jet diffuses away from the wall into cross flow. As the concentration of oxygen near the wall decreases when the cooling-jet velocity is reduced (decreasing M), the stoichiometric location moves closer to the wall as seen in Fig. 7. On the other hand, H_2 in the cross flow has to diffuse further toward the wall for finding enough oxygen. If the mass and heat diffusion rates were the same, then one would expect the heat also to conduct similarly and make the stoichiometric point to be at the same temperature. However, the diffusion of H_2 occurs at a much faster rate than the heat transport, which makes temperature to lag behind H_2. Consequently, temperature at the stoichiometric point did not reach to the same value when blowing ratio was decreased as seen in Fig. 7. By how much temperature decreases at stoichiometry will depend on the flow residence time, which is inversely proportional to the blowing ratio. Therefore, due to the differences in mass and heat transports (non-unity Lewis number), local temperature at stoichiometry decreases when the blowing ratio is decreased (residence time increased). Lower temperature at stoichiometry delays autoignition—hence, the flames at lower blowing ratios are established at locations further downstream.

The proposed hypothesis on the role of non-unity Lewis number in shifting the flame anchor location upstream with blowing ratio could be verified in the calculations through artificially changing the diffusion coefficients. Calculations for the flames in Fig. 5 are repeated after setting the diffusion coefficient of each species equal to the thermal conductivity of the local mixture. This eliminated the preferential diffusion for the species and set the mass diffusion equal to heat diffusion (Lewis number equal to unity). Resulted flame structures in the form of heat-release-rate and OH-concentration distributions and streamlines are shown in Fig. 8. Compared to the original simulations (Fig. 5) the modified calculations resulted in flames that are anchored closer to the slot. This is as expected since the diffusion of H_2 is artificially reduced for enforcing the unity-Lewis-number condition, which allowed the stoichiometry to establish at higher temperatures and, thereby, the autoignition to occur sooner (closer to the lot). All three flames in Fig. 8 are anchored at the same location ($x = 203.7$ mm) making the flame anchoring location independent of the blowing ratio. These calculations confirm that the differences in the mass and heat transports shifted the flame (Fig. 5) upstream as the blowing ratio is increased.

4.2. Effect of heat release

The incoming hot, fuel-rich combustion products are cooled by the sidewall prior to the slot and then by the cold injected air downstream of the slot. The latter cooling is not obvious in Fig. 5 due to the heat released from combustion. For understanding the extent of cooling provided in the film-cooling test rig, calculations have been repeated after replacing the air jet with a nitrogen jet and, thereby, suppressing the combustion processes. Cross-sectional variations of velocity and temperature at $x = 215$ mm with and without combustion are compared in Fig. 9a–c for the three blowing-ratio cases, respectively. Velocity component in the lengthwise direction (x) is shown in these figures. Broken lines labeled with air represent the cases with combustion. The weak nitrogen or air jet (injected at $x = 200$ mm) in the case of $M = 1$ has dissipated completely by the time it reached 215 mm and a smooth boundary-layer type velocity profile was established (Fig. 9a). Highly viscous combustion products in the boundary layer in the air-injection case retarded the flow in the boundary layer and, consequently, accelerated the flow in the freestream. Temperature profile shows a flame-like structure in the boundary layer. Interestingly, temperature near the top edge of the boundary layer ($3 < h < 4.2$ mm) dropped slightly below that obtained with N_2 injection. In fact, such drop in temperature was noted in all of the blowing-ratio cases, even though it is less significant at higher blowing ratios. The difference in heat and mass transport is responsible for this temperature behavior. Oxygen diffuses at a slower rate compared to the local heat transport where as, nitrogen diffuses at a rate close to that of heat. Therefore, replacing air jet with nitrogen made the temperature of the cross-flow gas to dissipate slowly. The variations in temperature arising from the differences in heat and mass transport decrease with flow velocity (blowing ratio) due to residence time as explained with respect to the flame base movement.

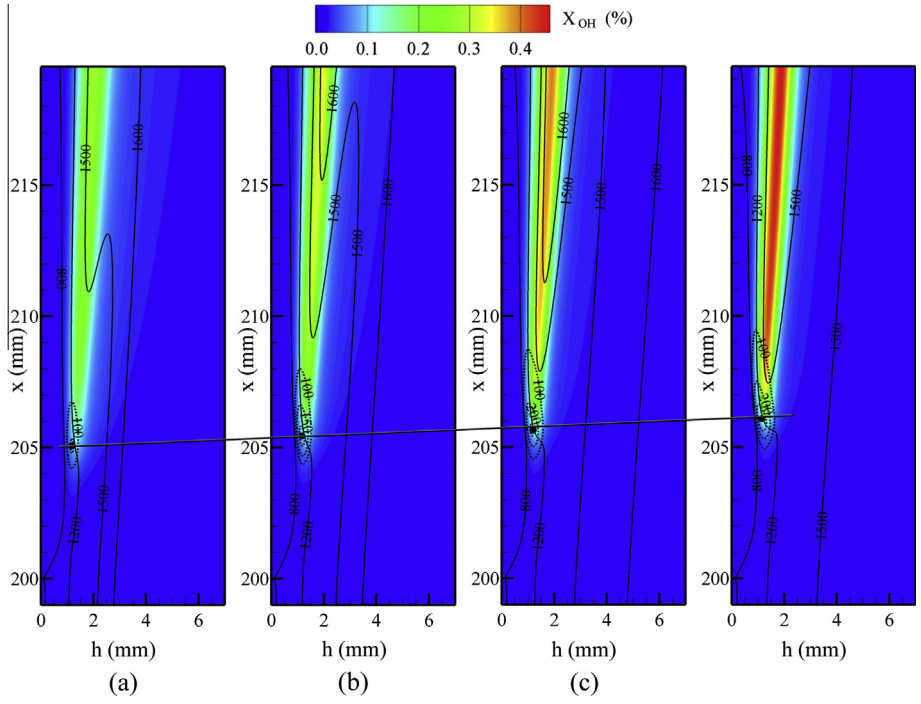

Fig. 10. Flames obtained for cross-flow equivalence ratios of (a) 1.4, (b) 1.5, and (c) 1.6 and for a blowing ratio of 4. Streamlines (solid lines) and iso-contours of heat release rate (broken lines) are superimposed on OH concentrations.

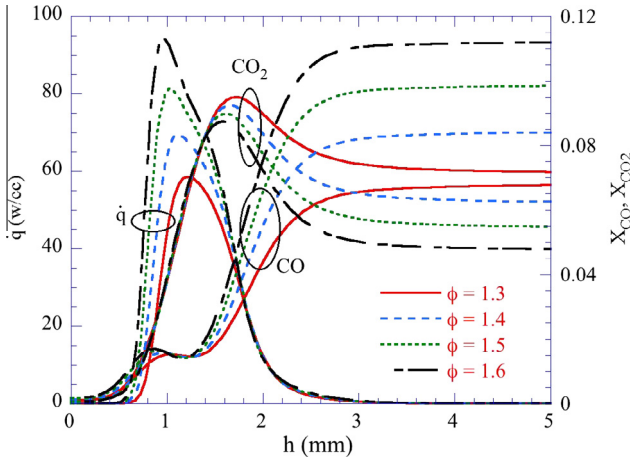

Fig. 11. Cross-sectional distributions (at $x = 210$ mm) of heat release rate and CO and CO_2 concentrations obtained at a blowing ratio of 7.

4.3. Effect of cross-flow equivalence ratio

Influence of fuel content in cross flow on the flame structure is studied through changing the equivalence ratio of the propane-air mixture fed into WSR. The composition of product gasses that enter the test section for different equivalence ratios are listed in Table 1 along with the measured temperatures. As expected, concentrations of fuels H_2 and CO increased with equivalence ratio. Calculations for the reacting flowfields in the test section are performed for all these equivalence ratios for blowing ratios 1, 4 and 7. Laminar flames computed for a blowing ratio of 4 with cross-flow equivalence ratios of 1.3, 1.4, 1.5 and 1.6 are shown in Fig. 10a–d, respectively. Streamlines and heat-release-rate contours are superimposed on OH-concentration distributions. Note that the flame in Fig. 10a for cross-flow equivalence ratio of 1.3 is identical to that shown in Fig. 5b. However, a larger color scale is used in Fig. 10 for covering wider range of OH concentrations. The peak OH concentration was nearly doubled when the equivalence ratio was increased from 1.3 to 1.6. Similarly, peak temperature (not shown in the plots) went up from 1784 K to 1972 K and heat release rate also increased. Cross-sectional distributions of heat release rate and CO and CO_2 concentrations at $x = 210$ mm are compared for different cross-flow equivalence ratios in Fig. 11.

Calculations in Fig. 10 suggest that the flame anchoring location shifted downstream with ϕ. This trend matches with that observed in the experiment (Fig. 3). A quick conclusion based on premixed flame theory could erroneously link the decreasing flame speed with increasing ϕ to the observed downstream shift in the flame anchor location. However, as discussed previously, increasing ϕ should be viewed as decreasing fuel dilution. As seen in Figs. 10 and 11, decreasing fuel dilution increases heat release rate. That means the intensely burning flame base at higher ϕ's should move its location upstream under the same flow conditions. This is not what happened to the flames in Fig. 10. In fact, the downstream shift in flame anchor location is resulting from the preferential-diffusion effects. Recall the roles of mass and heat transports in shifting the flame anchoring location when blowing ratio was increased (Fig. 5). Diffusive mass transport of hydrogen is faster than conductive heat transport. The increased amount of hydrogen in the higher-equivalence-ratio cross flow makes the temperature of the local mixture at stoichiometry to decrease further. Note that the flames in film cooling test rig are established through autoignition process. Decrease in the temperature of the fuel–air mixture delays autoignition process and shifts the ignition point to downstream location. Interestingly, calculations performed after setting diffusion of every species is equal to local thermal conductivity (similar to those in Fig. 8) resulted a slight upstream shift to the flame base when ϕ was increased. In the absence of preferential diffusion, the effect of fuel dilution became predominant and moved the flame base upstream as the flame burned more intensely in higher ϕ cases.

5. Summary and conclusions

OH-PLIF measurements in AFRL film-cooling rig suggested that the base of the flame shifts upstream with increase in blowing ratio for a fixed cross flow and shifts downstream with increase in equivalence ratio for a fixed blowing ratio. Both these trends are counterintuitive from jet diffusion flames' stability viewpoint. A time-dependent, detailed-chemistry CFD model was used for understanding this phenomenon. Calculations for the laminar-like flowfields in the test section were performed with detailed laminar transport models. A semi-detailed chemical-kinetics model involving 52 species and 544 reactions was incorporated into UNICORN code for the combustion of propane–air mixtures.

Calculations have predicted the experimentally observed shifts in flame base when the blowing ratio and equivalence ratio were changed independently. Detailed analyses of the flowfields revealed that the changes in flame anchoring location resulted from the preferential diffusion of species. The higher diffusive transport rate of hydrogen compared to the local heat transport causes hydrogen to move into cooler regions and, consequently, causes stoichiometry to occur at lower temperatures. This effect becomes more pronounced when the concentration of H_2 in the cross flow or the local residence time increases. As a flame establishes in the test section when the temperature of the stoichiometric mixture reaches autoignition value, shifting of hydrogen into cooler regions delays the formation of the flame. Consequently, higher ϕ and lower blowing ratio cases shifted the flame anchoring location downstream. Simulations performed after setting diffusive mass transport of each species equal to the conductive transport of temperature yielded flame anchoring location independent of blowing ratio and equivalence ratio—confirming the hypothesis proposed based on preferential diffusion.

The reacting flow simulations presented here brought out several important aspects of secondary flames formed in fuel-rich combustion products. Presence of H_2 in the products enhances preferential diffusion effects, which are normally ignored in the combustion of hydrocarbon fuels. As H_2 will be a major fuel species in the products generated from burning of fuel-rich mixtures of any hydrocarbon fuels, one must pay attention to preferential diffusion while understanding the secondary flames formed in these mixtures.

Acknowledgments

Financial support for this work was provided by the Air Force Contract #FA8650-12-C-2236 (Ms. Amy Lynch) and by the Air Force Office for Scientific Research (Dr. Chiping Li).

Appendix A. Supplementary material

Supplementary data associated with this article can be found, in the online version, at http://dx.doi.org/10.1016/j.fuel.2015.02.006.

References

[1] Sirignano WA, Liu F. Performance increases for gas-turbine engines through combustion inside the turbine. J Propul Power 1999;15(1):111–8.
[2] Briones AM, Zelina J, Katta VR. Flame stabilization in small cavities. AIAA J 2010;48(1):224–35.
[3] Zelina J, Shouse DT, Hancock RD. Ultra-compact combustors for advanced gas turbine engines. ASME paper IGTI-2004-GT-53155; 2004.
[4] Roquemore WM, Shouse DT, Burns D, Johnson A, Cooper C, Duncan B, et al. Trapped vortex combustor concept for gas turbine engines. 39th AIAA Aerospace Sciences Meeting and Exhibit, AIAA-2001-0483, Reno, NV; 2001.
[5] Hsu K-Y, Goss LP, Roquemore WM. Characteristics of a trapped-vortex combustor. J Propul Power 1998;14(1):57–65.
[6] Polanka MD, Zelina J, Anderson WS, Sekar B, Evans DS, Lin C-X, et al. Heat release in turbine cooling I: experimental and computational comparison of three geometries. J Propul Power 2011;27(2):257–68.
[7] Kirk DR, Guenette GR, Lukachko SP, Waitz IA. Gas turbine engine durability impacts of fuel-air ratio combustors–part II: near-wall reaction effects on film-cooled heat transfer. J Eng Gas Turbines Power 2003;125(3):751–9.
[8] Lukachko SP, Kirk DR, Waitz IA. Gas turbine engine durability impacts of high fuel-air ratio combustors—part I: potential for secondary combustion of partially reacted fuel. J Eng Gas Turbines Power 2003;125(3):742–50.
[9] Bohan BT, Blunck DL, Polanka MD, Kostka S, Jiang N, Stouffer SD. Impact of an upstream film-cooling row on mitigation of secondary combustion in a fuel rich environment. J Turbomach 2013;136(3) [031008-031008-8].
[10] Lin C-X, Holder RJ, Sekar B, Zelina J, Polanka MD, Thornburg HJ, et al. Heat release in turbine cooling II: numerical details of secondary combustion surrounding shaped holes. J Propul Power 2011;27(2):269–81.
[11] Mikofski M, Williams TC, Shaddix CR, Blevins LG. Flame height measurement of laminar inverse diffusion flames. Combust Flame 2006;146(1–2):63–72.
[12] Mikofski MA, Williams TC, Shaddix CR, Fernandezpello AC, Blevins LG. Structure of laminar sooting inverse diffusion flames. Combust Flame 2007;149(4):463–78.
[13] Shaddix CR, Williams TC, Blevins LG, Schefer RW. Flame structure of steady and pulsed sooting inverse jet diffusion flame. Proc Combust Inst 2005;30(1):1501–8.
[14] Katta VR, Blevins LG, Roquemore WM. Dynamics of an inverse diffusion flame and its role in polycyclic-aromatic-hydrocarbon and soot formation. Combust Flame 2005;2005(142):33–51.
[15] Partridge WP, Laurendeau NM. Nitric oxide formation by inverse diffusion flames in staged-air burners. Fuel 1995;74(10):1424–30.
[16] Clausing EM, Senser DW, Laurendeau NM. Peclet correlation for stability of inverse diffusion flames in methane-air cross flows. Combust Flame 1997;110(3):405–8.
[17] Partridge WP, Reisel JR, Laurendeau NM. Laser-saturated fluorescence measurements of nitric oxide in an inverse diffusion flame. Combust Flame 1999;116(1–2):282–90.
[18] Muppidi S, Mahesh K. Direct numerical simulation of passive scalar transport in transverse jets. J Fluid Mech 2008;598:335–60.
[19] Gutmark EJ, Ibrahim IM, Murugappan S. Dynamics of single and twin circular jets in cross flow. Exp Fluids 2011;50(3):653–63.
[20] Evans DS. The impact of heat release in turbine film cooling. MS Thesis, Air Force Institute of Technology, Dayton, OH; 2008.
[21] Stouffer SD, Pawlik R, Justinger G, Heyne J, Zelina J, Ballal D. Combustion performance and emissions characteristics for a well-stirred reactor for low volatility hydrocarbon fuels. In: 43rd AIAA/ASME/SAE/ASEE Joint Propulsion Conference, AIAA-2007-5663, Cincinnati, OH; 2007.
[22] Kostka S, Roy S, Lakusta PJ, Meyer TR, Renfro MW, Gord JR, et al. Comparison of line-peak and line-scanning excitation in two-color laser-induced-fluorescence thermometry of OH. Appl Opt 2009;48(32):6332–43.
[23] Roquemore WM, Katta VR. Role of flow visualization in the development of UNICORN. J Visual 2000;2(3/4):257–72.
[24] Katta VR, Goss LP, Roquemore WM. Numerical investigations of transitional H_2/N_2 jet diffusion flames. AIAA J 1994;32(1):84–94.
[25] Katta VR, Roquemore WM. AIAA J 1998;36(11):2044–54.
[26] Katta VR, Roquemore WM. Calculation of multidimensional flames using large chemical kinetics. AIAA J 2008;46(7):1640–50.
[27] <http://web.eng.ucsd.edu/mae/groups/combustion/sdmech/sandiego20091101_CK.txt>.
[28] Katta VR, Aggarwal SK, Roquemore WM. Evaluation of chemical-kinetics models for n-heptane combustion using a multidimensional CFD code. Fuel 2012;93:339–50.
[29] Katta VR, Goss LP, Roquemore WM. Simulation of vortical structures in jet diffusion flames. Int J Numer Method Heat Fluid Flow 1994;4(5):413–24.
[30] Bogard DG, Thole KA. Gas turbine film cooling. J Propul Power 2006;22:249–71.
[31] Takahashi F, Katta VR. Reaction kernel hypothesis for the stability limit of methane jet diffusion flames. Proc Combust Inst 2000;28:2071–8.
[32] Katta VR, Blunck D. Numerical studies on flames established in reacting film-cooling experiment. In: ASME Turbo Expo 2014: turbine technical conference and exposition, GT2014-25730, Dusseldorf, Germany, June 16–20, 2014.